^{13}C MRS: An Outstanding Tool for Metabolic Studies

TIAGO B. RODRIGUES,[1,2] SEBASTIÁN CERDÁN[1]

[1] *Instituto de Investigaciones Biomédicas "Alberto Sols" C.S.I.C./U.A.M., Madrid, Spain*
[2] *Departamento de Bioquímica, Centro RMN e Centro de Neurociências e Biologia Celular, Faculdade de Ciências e Tecnologia, Universidade de Coimbra, Coimbra, Portugal*

ABSTRACT: We provide an overview of ^{13}C magnetic resonance spectroscopy methods and their applications as an established metabolic tool with an emphasis on the use of high-resolution ^{13}C magnetic resonance spectroscopy and ^{13}C isotopomer analysis. Topics addressed include general properties of the ^{13}C magnetic resonance spectroscopy spectrum; different ^{13}C magnetic resonance spectroscopy acquisition protocols; determination of fractional ^{13}C enrichment, kinetic, or steady state measurements of metabolic flux; ^{13}C isotopomer analysis approaches; ^{13}C(^{2}H) magnetic resonance spectroscopy methodologies; and in vivo ^{13}C magnetic resonance spectroscopy. Some illustrative applications are described. © 2005 Wiley Periodicals, Inc. Concepts Magn Reson Part A 27A: 1–16, 2005

KEY WORDS: ^{13}C MRS; isotopic dilution; isotopomer analysis; tricarboxylic acid cycle; glutamine cycle; hydrogen turnover

INTRODUCTION

The first ^{13}C magnetic resonance spectroscopy (^{13}C MRS) study of a living organism was probably reported in 1972 (*1*). Authors followed the metabolism of (1-^{13}C) glucose by a eukaryotic cell system and concluded that the use of this pioneering technique "could have numerous applications for in vivo metabolic studies." Since then, ^{13}C MRS has developed steadily to a method routinely used in metabolic research with cells, perfused organs, animals, and even humans (*2–5*). This progress has been favored by the

ability of ^{13}C MRS to (i) perform repetitive, noninvasive measurements of metabolic processes as they proceed in their own intracellular environment and (ii) its capacity to measure unique physical properties not detectable by other methodologies, such as spin coupling patterns, isotopic shifts, or magnetic relaxation times T_1 and T_2. These properties have been shown to provide valuable information on the operation in situ of specific metabolic pathways or the dynamics of some important biological assemblies, exceeding in many cases the interpretations provided by previously used radioactive, spectrophotometric, or fluorimetric approaches.

^{13}C MRS allows detecting magnetic resonances from ^{13}C, the only stable isotope of carbon having a magnetic moment. The natural abundance for ^{13}C is roughly 1.1% of the total carbon and its magnetogyric ratio is approximately one-fourth of that of the proton. These two circumstances make ^{13}C MRS an insensitive technique (*6*). Despite this, natural abundance ^{13}C resonances from carbons of the fatty acid chains

of triglycerides are classically observed in most tissues, and glycogen carbons can be detected in the liver and muscle of fed animals and man (2, 3, 7). The sensitivity problem can be improved markedly by using ^{13}C enriched substrates. The combination of ^{13}C MRS detection and substrates selectively enriched in ^{13}C in specific positions have made it possible to follow in vivo and in vitro the activity of a large variety of metabolic pathways in cells, animals, and humans. These include glycolysis and the pentose phosphate pathway, glycogen synthesis and degradation, gluconeogenesis, the tricarboxylic acid cycle, ketogenesis, ureogenesis and the glutamate, glutamine, GABA cycle in brain, and others (see references [2–4] for reviews).

The design of ^{13}C MRS experiments with selectively ^{13}C-enriched substrates is similar to the classical radiolabeling experiments using ^{14}C. A relevant difference is that ^{13}C precursors are administered in substrate amounts, whereas ^{14}C substrates are used in tracer amounts. However, ^{13}C MRS presents important advantages over ^{14}C. First, the metabolism of the ^{13}C-labeled substrate can be followed in real time, in situ, and noninvasively (4, 5). Second, even if tissue extracts are prepared, the detection of ^{13}C in the different carbon resonances of a specific metabolite does not require separation and carbon by carbon degradation, a prerequisite in the experiments with radioactive ^{14}C (8). Finally, the analysis by ^{13}C MRS of homonuclear spin-coupling patterns and isotope effects allows investigation if two or more ^{13}C atoms occupy contiguous positions in the same metabolite molecule. The latter approach represents, as will be illustrated later in this article, an enormous gain in information as compared with the classical radioactive ^{14}C experiments (8). As a counterpart to these advantages, ^{13}C MRS is significantly less sensitive than other conventional metabolic techniques, such as radioactive counting, mass spectrometry, and spectrophotometric or fluorimetric methods.

The purpose of this article is to provide an introduction to ^{13}C MRS methods and applications with particular reference to high-resolution ^{13}C NMR and ^{13}C isotopomer approaches. The methodology described here refers mainly to studies performed with tissue extracts but provides an adequate framework to understand the approaches used with in situ animals and human beings. More information on the latter aspects may be found in references (9–12) or in *NMR in Biomedicine*'s 2003 special issue titled "^{13}C NMR Studies of Cerebral Metabolism." Other reviews cover in more detail the metabolic information derived from ^{13}C isotopomer analysis in the adult mammalian brain (13) or in primary cultures of neural cells (14, 15).

METHODOLOGY

The ^{13}C MRS Spectrum: Spin Coupling Patterns and Isotopic Shifts

^{13}C resonances are distributed over a large chemical shift range and experience low relaxation rates (16). Normally, high-resolution ^{13}C MRS spectra of metabolites depict a collection of well-resolved narrow resonances distributed over large chemical shift range ($\sim$ 250 ppm), even in viscous media as those found in vivo.

Figure 1 shows typical proton-decoupled ^{13}C MRS spectra of perchloric acid extracts obtained from the brain of rats infused with $(1,2-^{13}C_2)$ glucose [see Fig. 1(A)] or $(1,2-^{13}C_2)$ acetate [see Fig. 1(B)] as compared with the natural abundance ^{13}C MRS spectrum of a rat infused with unlabeled glucose (17). The most important resonances detected are those from the carbons of glutamate, glutamine, GABA, NAA, inositol, and glucose. The increased intensity of the resonances observed in the upper panels clearly indicates that the ^{13}C label has been incorporated in cerebral metabolites. Indeed, the difference between the intensity of the natural abundance signal and the total intensity of the corresponding multiplet resonance in the spectrum obtained with ^{13}C-labeled substrate reveals the net amount of ^{13}C incorporated in the corresponding carbon. Most of the resonances observed in the upper panel of Fig. 1 depict an apparent triplet structure produced by homonuclear ^{13}C-^{13}C coupling. These pseudotriplets are derived from the superposition of doublets originated in those metabolites containing two contiguous ^{13}C atoms in the same molecule or from singlets, corresponding to those metabolites containing the ^{13}C atom bonded to ^{12}C neighbors.

Figure 2 and reference (13) illustrate more clearly these aspects. If pathway A incorporates one ^{13}C atom from the labeled substrate in position i of metabolite M, a singlet resonance will appear at frequency ω_i. If by any chance the ^{13}C atom from the substrate is incorporated through a different mechanism (pathway B) in position i + 1 of M, a new singlet resonance will appear, now located at a different frequency ω_{i+1} in the ^{13}C MRS spectrum. It becomes then possible to determine the relative contributions of pathways A and B to the formation of M by the relative intensities of the ^{13}C resonance at ω_i to that of ω_{i+1}. If pathways A and B are both active, ^{13}C atoms may be incorporated simultaneously at positions i and i + 1 of the
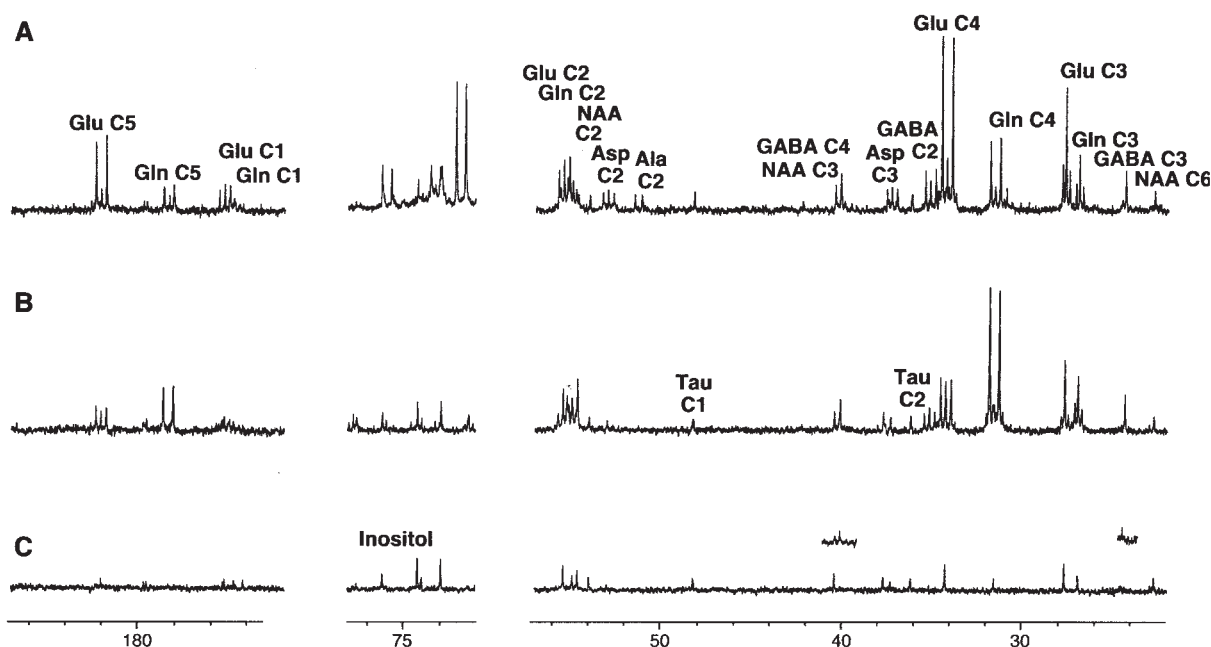
**Figure 1** ^{13}C MRS spectra (90.55 MHz, 22 °C, pH 7.2) of brain extracts after infusion of (1,2-^{13}C$_2$) glucose (A), (1,2-^{13}C$_2$) acetate (B), or unlabeled glucose (C). Gln C3 (26.87, $^1J_{23}$ = $^1J_{34}$ = 34.5), Glu C3 (27.80, $^1J_{23}$ = $^1J_{34}$ = 34.5), Gln C4 (31.60, $^1J_{34}$ = 34.5, $^1J_{45}$ = 49.0), Glu C4 (34.16, $^1J_{34}$ = 34.5, $^1J_{45}$ = 51.0), GABA C2 (35.07, $^1J_{12}$ = 51.0), Gln C2 (55.0, $^1J_{12}$ = 54.96, $^1J_{23}$ = 34.5), Glu C2 (55.35, $^1J_{12}$ = 53.0, $^1J_{23}$ = 34.5). Numbers in parenthesis give the chemical shift in ppm, followed by the geminal coupling constant(s) in Hz. Insets in C: Natural abundance contribution of unlabeled GABA in the spectra of vigabatrin treated animals. Ala: alanine, Asp: aspartate, GABA: γ-aminobutyric acid, Gln: glutamine, Glu: glutamate, NAA: N-acetylaspartate, Tau: taurine. Reproduced from (*17*) with permission of the publisher.

same metabolite molecule. In this case, a new interaction appears between the adjacent magnetic moments of contiguous ^{13}C nuclei. This interaction splits the original singlet resonances into doublets. This is so because the multiplicity of ^{13}C resonance coupled to nucleus X is given by the rule 2nI + 1, where n is the number of X nuclei coupled to ^{13}C, and I is their angular momentum (I = 1/2 for X = ^{1}H, ^{31}P, ^{13}C, ^{15}N or I = 1 for X = ^{2}H). This interaction is known as homonuclear scalar coupling and is transmitted through the electrons of the ^{13}C-^{13}C-bond.

^{13}C MRS Acquisition: ^{1}H Decoupling and NOE Enhancement

Figure 3 illustrates the most important characteristics of ^{13}C MRS data acquisition and the resulting ^{13}C MRS spectra for the hypothetical case of a ^{13}C carbon bonded only to a vicinal proton. Spin coupling to one or more protons complicates the interpretation of the ^{13}C spectra and thus it is normally removed using a variety of proton decoupling techniques. All decoupling procedures are based on the same principle, the

broadband irradiation of all proton resonances with a high-power amplitude-modulated and monochromatic ^{1}H frequency. The irradiation saturates the Boltzman energy levels of the proton spectrum, removing the macroscopic magnetization of all protons and making the scalar proton couplings disappear from the ^{13}C spectrum. There are two main proton decoupling methods: broad band decoupling (BB) and composite pulse decoupling (WALTZ). They differ in the type of modulation of the proton frequencies. Whereas BB uses a continuous irradiation of proton frequencies with a train of rectangular pulses of identical duration and opposite phase (*16*), composite pulse decoupling uses blocks of ^{1}H pulses of different pulse lengths and phases (*18*). WALTZ sequences are more efficient than BB, allowing decoupling ^{13}C spectra using less decoupler power and diminishing also the potential dielectric heating of the sample. In addition to the removal of scalar ^{1}H couplings, ^{1}H irradiation can cause an increase in the ^{13}C signal intensity because of the nuclear overhauser enhancement effect (NOE). The NOE effect is a magnetization transfer process from ^{1}H to ^{13}C, which may increase the
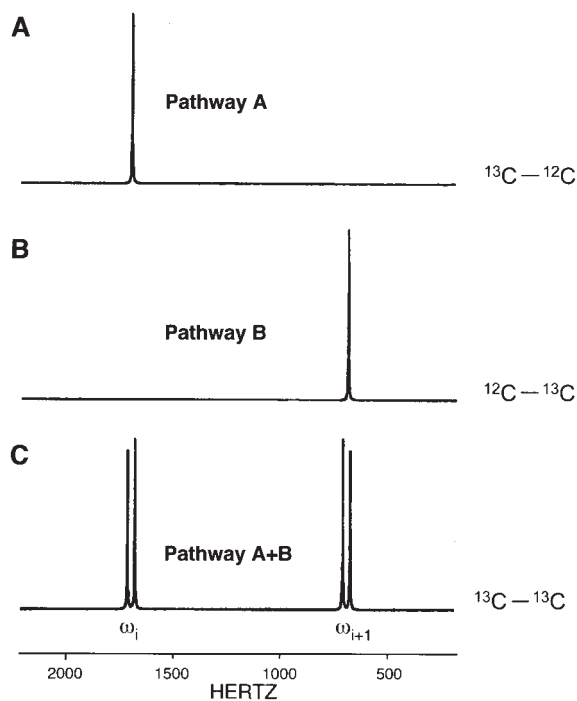
Figure 2   Homonuclear coupling patterns in two contiguous carbons of the same metabolite molecule. (A) ^{13}C-^{12}C; (B) ^{12}C-^{13}C; (C) ^{13}C-^{13}C.

intensity of a ^{13}C resonance up to threefold in favorable cases. More information on decoupling sequences and NOE enhancement in ^{13}C MRS is given in the classical monograph by Breitmeier and Voelter (16).

Different decoupling schemes are possible that produce proton-coupled or proton-decoupled ^{13}C MRS spectra containing (or not containing) NOE enhancement. If the ^{1}H decoupler is not used in conjunction with ^{13}C excitation (see Fig. 3, top panel), a proton-coupled ^{13}C spectrum is obtained. The multiplet structure of the proton-coupled ^{13}C resonance depends of the number of protons coupled to the observed carbon and follows the rule, $2nI + 1$. For $n = 1$, a doublet is obtained. If the decoupler is gated only during the acquisition of the ^{13}C FID (inverse gated decoupling), a proton-decoupled spectrum devoid of NOE is obtained. On the contrary, if the decoupler is gated only during the relaxation delay and not during the acquisition (direct gated decoupling), a proton-coupled NOE-enhanced ^{13}C spectrum is obtained. Inverse-gated decoupling avoids the effects of NOE, whereas direct-gated decoupling generates ^{1}H-coupled ^{13}C spectra with complete NOE enhancement. Decoupling during the complete cycle time generates a proton-decoupled NOE-enhanced ^{13}C spectrum (19).

A different strategy was proposed in 1985 by Rothman et al. (20). These authors showed that ^{13}C-labeled metabolites could be detected in vivo with ^{1}H sensitivity using a ^{13}C decoupling sequence in con-
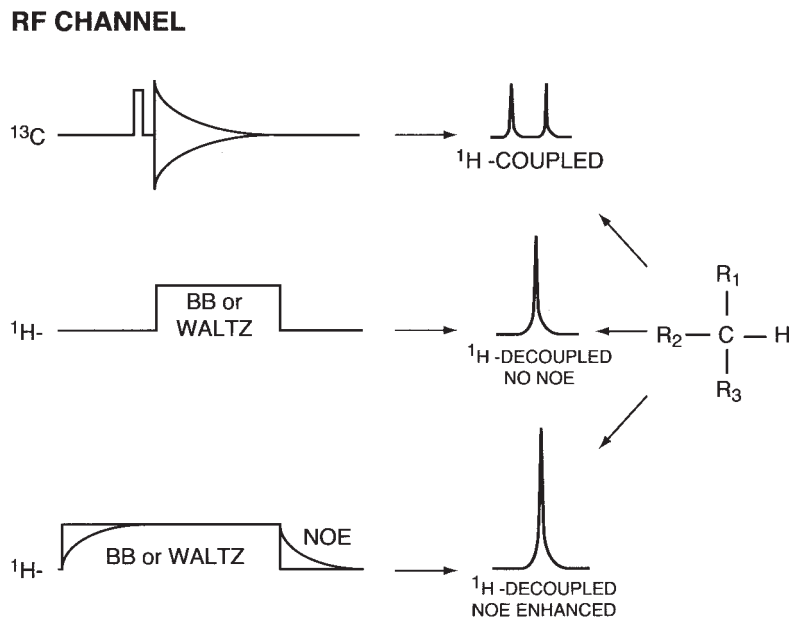
Figure 3   Acquisition of ^{13}C MRS spectra under different ^{1}H-decoupling conditions. Top: proton-coupled ^{13}C MRS spectrum; middle: proton-decoupled ^{13}C MRS spectrum without NOE; bottom: proton-decoupled ^{13}C MRS spectrum with NOE. The ^{13}C or ^{1}H symbols at the left of every sequence indicate RF transmitter or decoupler pulses, respectively.

junction with ^{1}H detection (POCE; proton observed carbon edited). Since then, this approach has been used successfully in vivo and in vitro, and several examples are available in the literature (*21, 22*).

^{13}C MRS Quantitation

The interpretation of ^{13}C MRS spectra in terms of flux through metabolic pathways requires the quantitation of the ^{13}C incorporated in specific carbons. This is normally done by expressing ^{13}C incorporation as a fractional ^{13}C enrichment in carbon C_i (YC_i). The fractional ^{13}C enrichment YC_i is defined as the amount of ^{13}C relative to the total carbon (^{13}C+^{12}C) present in C_i.

$$YC_i = \frac{^{13}C \ concentration \ in \ C_i}{(^{13}C + {}^{12}C) \ concentration \ in \ C_i} \quad [1]$$

The measurement of YC_i involves (i) the determination of ^{13}C concentration by ^{13}C MRS methods and (ii) the measurement of the total carbon concentration by more conventional techniques (automatic ion exchange chromatography for amino acids, HPLC, enzymatic end point methods for other metabolites, and so on).

Special precautions must be taken in the determination of the concentration of ^{13}C in C_i by ^{13}C MRS because ^{13}C signal intensities depend on various factors, in addition to the ^{13}C concentration. Thus, ^{13}C resonances from carbons with the same ^{13}C concentration may have different intensities or areas depending on the particular pulsing condition used, the relaxation behavior of the observed carbon, its NOE effect, and acquisition and repetition times.

The intensity, area, or magnetization $M(t)$ of a ^{13}C carbon resonance is given by Eq. [2] (*23*):

$$M(t) = M(0)\frac{(\sin \Phi)(e^{t/T_1} - 1)}{(e^{t/T_1} - 1)}$$
$$+ (\eta + 1)(1 - e^{-a/T_1})e^{-t/T_1} \quad [2]$$

where $M(t)$ is the area of the resonance under the pulsing conditions used, $M(0)$ is the area of the resonance under equilibrium magnetization conditions, Φ is the flip angle used in the ^{13}C pulse, η is the NOE enhancement factor, t is the total cycle time, T_1 is the longitudinal relaxation time, and a is the acquisition time. $M(0)$ is proportional to the concentration of ^{13}C. Thus, if the ^{13}C spectrum is acquired under fully relaxed conditions, a comparison of the area $M(0)$ in the sample with the area of the same resonance in a standard solution of known concentration would give a value for the ^{13}C concentration in the sample. In practice, this procedure is not recommended because T_1 values of ^{13}C in extracts vary from approximately 3 s in methyl and methylene resonances to 30 s or more in quaternary carbons like those of carboxylic acids. Thus to recover completely the equilibrium magnetization $M(0)$ in the sample, the slowest carbons would require a total cycle time of approximately 150 s. This is incompatible with reasonable acquisition times. Thus, a compromise is normally adopted and $M(0)$ in the sample and standard solutions can be calculated from $M(t)$ measured under partially saturating conditions (3–6 s total cycle time) and predetermined values of T_1 and Φ using the equation described above. To favor quantitation, the influence of the NOE factor is avoided using gated decoupling sequences.

Other ^{13}C MRS quantitation strategies may be used to determine fractional ^{13}C enrichments: (i) direct comparison of the areas of the ^{13}C resonances in the sample spectrum with those of the same resonances in the spectrum of a standard solution of known concentration acquired under identical pulsing conditions; (ii) comparison of the intensities of ^{13}C resonances in the sample spectrum with the intensity of the natural abundance signals (1.1% YC_i) from an experiment performed using an unlabeled substrate; and (iii) use of ^{1}H MRS to measure the relative area of the ^{13}C satellites to the total area of the ^{1}H resonance (see below). Once the ^{13}C concentration is known, the fractional ^{13}C enrichment can be calculated and used in mathematical models of metabolism to determine metabolic flux.

DETERMINATION OF METABOLIC FLUX BY ^{13}C MRS

Kinetic and Steady-State Methods

The main goal of ^{13}C MRS studies is to explore qualitatively or quantitatively metabolic flux through a specific step in a pathway, through a whole pathway, or through a combination of several pathways. To measure metabolic flux by in vivo ^{13}C MRS, a ^{13}C-enriched precursor is administered (infused, perifused, and injected) to the biological system. After its administration, ^{13}C atoms from the substrate substitute progressively, because of metabolism, the ^{12}C atoms previously present in the system. This substitution may be monitored kinetically in some favorable cases by ^{13}C MRS techniques (*24–27*).

Once the kinetics of ^{13}C enrichment are known it becomes possible to fit the time course of ^{13}C enrich-
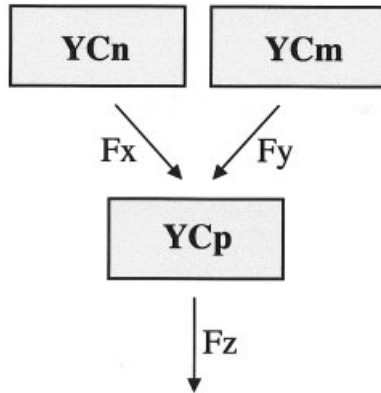
Figure 4   Principles of mass conservation and isotope conservation at steady state. YCn, YCm, and YCp refer to fractional ^{13}C enrichments in carbons Cn, Cm, and Cp. Fz or Fx and Fy refer to metabolic fluxes leaving and entering the Cp pool, respectively. Mass conservation principle: Fz = Fx + Fy. Isotope conservation principle: YCp.Fz = YCn.Fx + YCm.Fy. If Fz is known, Fx and Fy can be calculated if YCp, YCm, and YCn are measured by ^{13}C MRS.

ment(s) to a metabolic model containing the fractional ^{13}C enrichment(s) as the dependent variable(s), time as the independent variable, and the unknown fluxes as the parameters to be fitted. This approach allowed calculating the flux through the tricarboxylic acid cycle and the glutamine cycle in the brain of animals and man (9, 25, 26).

Eventually, an isotopic steady state is achieved after continuous administration of a ^{13}C-enriched substrate. Under steady-state conditions, the rate of incorporation of ^{13}C equals the rate of disappearance, and principles of conservation of mass and isotope are fulfilled (Fig. 4).

These principles state that the total amount of carbon (^{13}C + ^{12}C) and the amount of ^{13}C entering a carbon pool are equal to the total amount of carbon (^{13}C + ^{12}C) and ^{13}C leaving the pool, respectively. It is possible then to set up a series of simultaneous equations relating the fractional ^{13}C enrichments determined in every carbon to input output fluxes (see Fig. 4). The unknown fluxes can be found, provided the number of equations is equal to the number of unknowns. This is many times the limiting condition as the number of fractional ^{13}C enrichments determined by ^{13}C MRS or directly measurable fluxes by other conventional methods is small in comparison with the complexity of metabolic transformations investigated. In these cases, the use of simplified models of metabolism has proven to be useful. Examples of the steady-state approach based of isotopic dilution

can be found in the classic work of Chance et al. (27) or studies of neural cell metabolism (28, 29).

The ^{13}C Isotopomer Approach

The methods based exclusively on the determination of fractional ^{13}C enrichment neglect the information provided by spin coupling patterns (see Fig. 2), resulting in a significant loss of information. Thus, for a five-carbon metabolite such as glutamate, ^{13}C enrichment determinations would produce at most five different enrichment values, one for every carbon. These number enrichments would support at most five input-output equations as described in Fig. 4.

The gain in information introduced by the use of spin coupling patterns or isotopic shifts is more easily perceived with the following example. For a molecule such as glutamate containing five carbons, five hydrogens, four oxygens, and one nitrogen atom, the possibilities of isotopic substitution with ^{13}C, ^{2}H, ^{17}O, and ^{15}N isotopes are large (Table 1). Glutamate has 32 possibilities of ^{13}C labeling. Each of these possibilities is an isotopic isomer (or isotopomer) of glutamate with 32 possibilities of deuteration, four possibilities of ^{17}O (or ^{18}O) labeling, and two possibilities of nitrogen substitution. Thus, a total of 32,768 isotopomers of (^{13}C, ^{2}H, ^{17}O, ^{15}N) glutamate are available for labeling in multinuclear studies. Fortunately, not all of these isotopomers are directly detectable by conventional ^{13}C MRS methods. Only about 40 isotopomers of (^{2}H,^{13}C) glutamate are easily detected in 1D ^{13}C MRS with combined ^{13}C and ^{2}H labeling; more would be detectable using more sophisticated 2D or 3D multinuclear MRS techniques. Input-output equations for each of these isotopomers can be written and solved, allowing a significantly larger number of fluxes to be determined than with the conventional fractional enrichment method. However, the large number of equations demands the use of computer programs to calculate and fit simulated ^{13}C spectra to

Table I   Possibilities of Isotopic Substitution in Glutamate

Atom	Number	Isotopic Substitution	Possibilities of Isotopic Labeling (Isotopomers)
Carbon	5	^{13}C	32
Hydrogen	5	^{13}C, ^{2}H	1,024
Oxygen	4	^{13}C, ^{2}H, ^{17}O(^{18}O)	16,384
Nitrogen	1	^{13}C, ^{2}H, ^{17}O(^{18}O), ^{15}N	32,768

experimental ones. At least two algorithms are available that perform this task, TCASIM (30) and METASIM (31). The isotopomer approach was initially developed for the estimation of the contribution of anaplerotic fluxes to the tricarboxylic acid cycle of the heart (32) and has been extended to the study of metabolic compartmentation in heart (33–36) and brain (13, 28, 37–41). In addition, ^{2}H-^{13}C couplings have been used in the study of solvent exchange reactions in the perfused liver (42, 43), and ^{15}N-^{13}C and ^{1}H-^{15}N couplings in the analysis of ammonia detoxification pathways (44, 45).

APPLICATIONS

Cerebral Metabolic Compartmentation as Revealed by the Use of Substrates Multiply Enriched in ^{13}C and High-Resolution ^{13}C MRS

A significant number of studies of cerebral metabolic compartmentation have used high-resolution ^{13}C MRS analysis of brain extracts and glucose or acetate contiguously labeled with ^{13}C as cerebral substrates (13, 17, 31, 37–41). An important basis for the use of this approach is the impressive amount of metabolic information contained in homonuclear spin coupling patterns.

Figure 5 provides an adequate frame to discuss these aspects by showing schematically the cerebral metabolism of (1,2-^{13}C$_2$) glucose or (1,2-^{13}C$_2$) acetate and their effects on ^{13}C MRS spectra of brain extracts. (1,2-^{13}C$_2$) glucose is transported from plasma to brain cells through glucose transporters and degraded directly to an equimolar mixture of (2,3-^{13}C$_2$) and unlabeled pyruvate through the Embden-Meyerhoff pathway. Cytosolic (2,3-^{13}C$_2$) pyruvate can be reduced to (2,3-^{13}C$_2$) lactate, transaminated to (2,3-^{13}C$_2$) alanine, or transported to the mitochondria for oxidative metabolism (46). In the mitochondrial matrix, (2,3-^{13}C$_2$) pyruvate can enter the tricarboxylic acid cycle through pyruvate dehydrogenase as (1,2-^{13}C$_2$) acetyl-CoA or through pyruvate carboxylase as (2,3-^{13}C$_2$) oxalacetate. In the first turn, (1,2-^{13}C$_2$) acetyl-CoA produces (4,5-^{13}C$_2$) α−ketoglutarate, while (2,3-^{13}C$_2$) oxalacetate forms (1,2-^{13}C$_2$) α−ketoglutarate. The exchange between α-ketoglutarate and glutamate, through aspartate aminotransferase, has been traditionally assumed to be fast compared with the tricarboxyxlic acid flux, and thus glutamate labeling is thought to reflect accurately the labeling in the α-ketoglutarate precursor (22). Thus (4,5-^{13}C$_2$) and (1,2-^{13}C$_2$) glutamate reflect ^{13}C labeling of the corresponding α-ketoglutarate precursors. (4,5-^{13}C$_2$) and (1,2-^{13}C$_2$) glutamate may produce (4,5-^{13}C$_2$) and (1,2-^{13}C$_2$) glutamine through glutamine synthase or (1,2-^{13}C$_2$) and (4-^{14}C) GABA through glutamate decarboxylase, respectively. If (4,5-^{13}C$_2$) or (1,2-^{13}C$_2$) α-ketoglutarate continue metabolism through the cycle, equimolar mixtures of (3,4-^{13}C$_2$) and (1,2-^{13}C$_2$) or (1-^{13}C) and (4-^{13}C) succinates, fumarates, and malates are produced, entering eventually a new turn of the cycle. Several studies of cerebral metabolism used (1,2-^{13}C$_2$) acetate as substrate (37–40). (1,2-^{13}C$_2$) acetate is believed to be transported and activated to (1,2-^{13}C$_2$) acetyl-CoA only in glial cells, bypassing the pyruvate dehydrogenase and pyruvate carboxylase steps of entry into the tricarboxylic acid cycle.

These ^{13}C labeling patterns are adequately reflected in the high-resolution ^{13}C MRS spectra of brain extracts by the intensities and multiplicities of the ^{13}C resonances from the individual carbons of glutamate, glutamine, and GABA. This is illustrated in Fig. 1, which shows representative ^{13}C MRS spectra obtained from brain extracts after metabolism of (1,2-^{13}C$_2$) glucose (A), of (1,2-^{13}C$_2$) acetate (B), or of unlabeled glucose (bottom). At steady state, glutamate carbons C4 (34.2 ppm) and C5 (182.2 ppm) reflect labeling of acetyl CoA carbons C2 and C1, whereas glutamate carbons C1 (175.5 ppm), C2 (55.5 ppm), and C3 (27.7 ppm) reflect labeling in oxalacetate carbons C4, C3, and C2, respectively. The relative proportions of (2,3-^{13}C$_2$) pyruvate entering the tricarboxylic acid cycle through pyruvate dehydrogenase or pyruvate carboxylase can be estimated by the relative intensities of the doublet resonances observed in the glutamate C4 and C2 carbons, respectively (47, 48).

In addition, ^{13}C MRS spectra of brain extracts provide an excellent tool to study cerebral metabolic compartmentation. This is more easily accomplished through the analysis of the homonuclear spin coupling patterns. Indeed, most of the observed resonances in Fig. 1 display an apparent triplet structure derived from the superposition of doublets and singlets. Doublets arise from contiguously ^{13}C-labeled isotopomers of glutamate, glutamine, and GABA, whereas singlets are derived from the corresponding isotopomers with ^{13}C carbons having only ^{12}C neighbors. The presence of cerebral compartmentation is easily demonstrated through the analysis of the glutamate and glutamine C3 and C4 carbon resonances. When (1,2-^{13}C$_2$) glucose is the substrate, the different singlet/doublet ratio in the glutamate and glutamine C3 carbons is inconsistent with a single pool of acetyl-CoA and oxalacetate condensing at the citrate synthase step of a unique cerebral tricarboxylic acid cycle. Similarly, when (1,2-^{13}C$_2$) acetate is the substrate, the singlet/
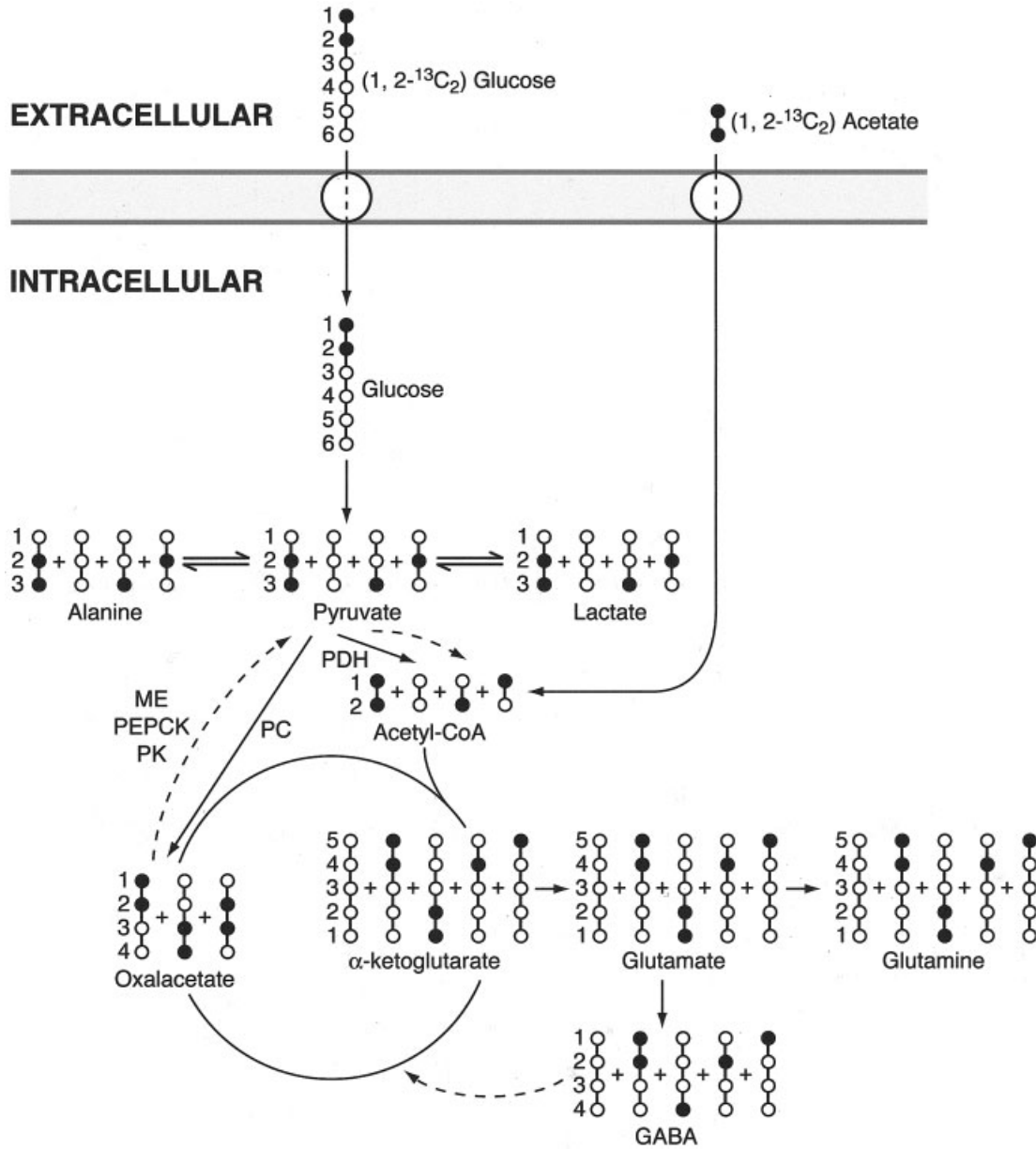
Figure 5 Cerebral metabolism of $(1,2-^{13}C_2)$ glucose and $(1,2-^{13}C_2)$ acetate. Filled circles indicate ^{13}C. Empty circles indicate ^{12}C. Only the first turn of the tricarboxylic acid cycle is considered. Contiguously labeled isotopomers of glutamate, glutamine and GABA originate the doublet resonances observed in Fig. 1. Single-labeled and natural abundance isotopomers originate singlet resonances in Fig. 1. PDH: pyruvate dehydrogenase, PC: Pyruvate carboxylase, ME: malic enzyme, PEPCK: phosphoenolpyruvate carboxykinase, PK: pyruvate kinase. Reproduced from (*13*) with permission of the publisher.

doublet ratio in glutamine C4 is clearly different from that of its precursor glutamate C4, a result inconsistent with the presence of a unique glutamate pool. This difference led to the description of the cerebral pyruvate recycling system, a pathway transforming $(1,2-^{13}C_2)$ acetyl-CoA units in $(1-^{13}C)$ and $(2-^{13}C)$ acetyl-CoA units, which occurs mainly in the synaptic terminals (*37, 49*). More quantitative interpretations can also be per-

formed with the help of programs for computer-assisted interpretations of ^{13}C MRS spectra (*13, 31*).

Hydrogen Turnover as Studied by ^{13}C MRS

As described previously, several ^{13}C MRS techniques have been implemented to study the turnover of indi-
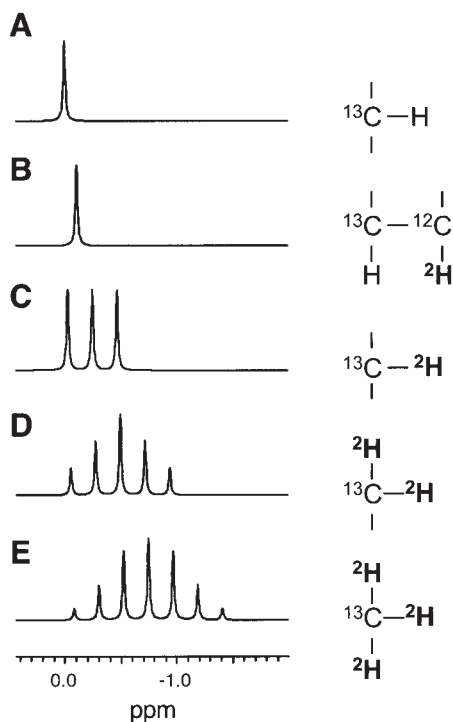
Figure 6 ^{2}H-^{13}C multiplets and deuterium-induced isotopic shifts in proton-decoupled ^{13}C MRS spectra. (A) preprotonated carbon, (B) vicinal deuteration, (C–E) geminal deuteration by one, two, or three deuterons. Simulations were performed with the program WINDAISY using the following parameters: $^1J_{C–H}$ = 20.06 Hz; geminal isotopic shift, Δ_1 = −22.89 Hz/deuteron; vicinal isotopic shift, Δ_2 = −9.89 Hz/deuteron. Reproduced from (50) with permission of the publisher.

vidual metabolite carbons by using precursors selectively enriched in ^{13}C. Because most metabolite carbons are attached to one or more hydrogen atoms, ^{13}C MRS could also serve as a valuable tool to analyze hydrogen turnover. This is a much faster process than ^{13}C turnover and therefore allows studying faster reactions. Our laboratory has proposed a double-labeling strategy to investigate hydrogen turnover. Our approach follows by ^{13}C MRS the exchange of pre-existing ^{1}H by ^{2}H at the steady state, when metabolism occurs in media containing a ^{13}C-labeled substrate and ^{2}H$_2$O (40, 42, 43, 50–52). This is possible because high-resolution ^{13}C MRS is well suited to detect complex deuteration patterns in ^{13}C-labeled metabolites.

The presence of one or more deuterons geminally or vicinally bound to the observed ^{13}C implies the appearance of characteristic ^{2}H isotopic shifts and ^{2}H-^{13}C couplings (50, 51, 53). Therefore, coupling patterns to ^{2}H may appear as splitted and/or shifted resonances in relation to the preprotonated ^{13}C reso-

nance. Figure 6 depicts this behavior. If one of the protons directly bonded to ^{13}C is substituted by ^{2}H, the original resonance is splitted into a 1:1:1 triplet (19.21 < $^1J_{C–H}$ < 22 Hz), inducing a geminal upfield isotopic shift (−0.25 < Δ_1 < −0.33 ppm). Two or three deuterons bound to the same ^{13}C atom would result in additive isotopic shifts and ^{2}H-^{13}C couplings patterns of five or seven line multiplets, shifted by −0.5 or −0.75 ppm, respectively. Even a vicinal deuterium substitution induces smaller and additive upfield isotopic shifts (−0.03 < Δ_2 < −0.11 ppm). Vicinal couplings to deuterium are too small to be resolved, and resonances shifted vicinally maintain the multiplet structure of their geminal couplings. Thus high-resolution ^{13}C MRS allows determining the number of deuterium replacements, their relative contributions, and their geminal or vicinal location with respect to the observed ^{13}C carbon of a specific ^{13}C isotopomers through the analysis of shifted and unshifted (^{1}H,^{2}H)^{13}C multiplets.

This kind of approach makes it possible to develop novel procedures to investigate and resolve in time fast metabolic processes, as long as they involve exchange of hydrogens by deuters. In our laboratory, we have monitored the dynamics of exchange from specific hydrogens of hepatic glutamate and aspartate with deuters from intracellular heavy water. With this approach it became possible to observe directly α-ketoglutarate/glutamate exchange and oxalacetate/aspartate exchange and subcellular compartmentation, by following in a time-resolved manner the sequence of events involved in the traffic of these metabolites through mitochondria and cytosol (42). In this work, the determination of relative (^{1}H,^{2}H,^{13}C) isotopomer populations is conveniently accomplished using a simulation program, which allows the quantitative determination of the relative contributions of the individual (^{1}H,^{2}H)^{13}C multiplets. Figure 7 shows a representative deconvolution of the C2 carbon resonance of (2-^{13}C) glutamate. Deconvolution of the C2 carbon resonance revealed contributions from five different (^{1}H,^{2}H,^{13}C) glutamate isotopomers. Notably, these results reveal intracellular glutamate compartmentation and slow α-ketoglutarate/glutamate exchange, a circumstance not considered previously.

Figure 8 illustrates the kinetics of deuteration of the H2 and H3 hydrogens from (2-^{13}C) glutamate during perfusions with (3-^{13}C) alanine in Krebs-Ringer bicarbonate (KRB) buffer containing 50% ^{2}H$_2$O. The faster timescale of hydrogen exchange allows resolving in time cytosolic deuteration, as those of (2-^{13}C, 3-^{2}H) glutamate, and mitochondrial deuterations, as that of (2-^{13}C, 3,3′-^{2}H$_2$) glutamate (42).
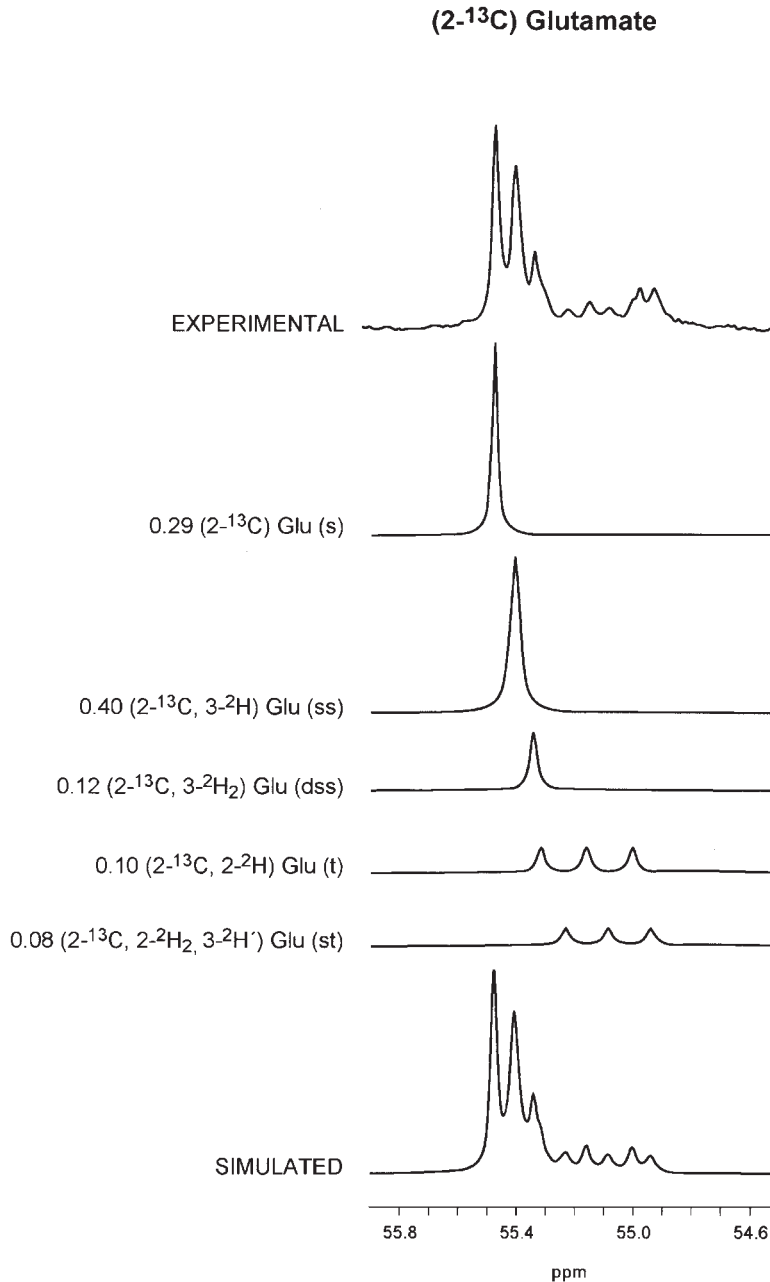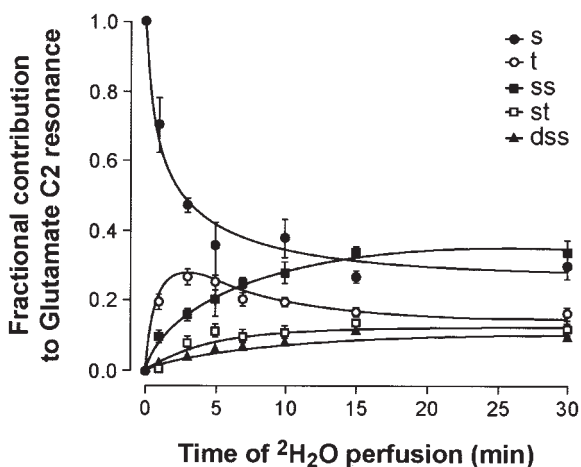
(2-^{13}C) Glutamate

Figure 7 Representative deconvolution of the C2 carbon resonances from (2-^{13}C) glutamate into the contributions of individual (^{1}H,^{2}H)^{13}C multiplets. ^{13}C MRS spectra (150.90 MHz, 22°C, pH 7.2) were obtained from the extracts of single livers perfused with 6 mM (3-^{13}C) alanine in 50% ^{2}H$_2$O for 15 min (C2 glutamate). Relative contributions of specific isotopomers are given as the fractional contribution of the corresponding multiplet to the total area of the analyzed resonance taken arbitrarily as one. Simulations were performed with the WINDAISY program. s: singlet, ss: shifted singlets, dss: doubly shifted singlet, t: triplet, st: shifted triplet. Reproduced from (*42*) with permission of the publisher.

In Vivo ^{13}C MRS and Clinical ^{13}C MRS

The possibility to obtain ^{13}C MRS spectra of metabolism as it proceeds in its own intracellular environment, in animal models or in human beings, represents one of the most attractive possibilities of the ^{13}C MRS method. Although ^{13}C MRS can be performed in natural abundance conditions, studies with administration of exogenous ^{13}C-enriched precursors are more common. If a ^{13}C label is delivered adequately to an in vivo system, the incorporation of the ^{13}C label

Figure 8 Kinetics of deuteration of the H2 and H3 hydrogens from (2-^{13}C) glutamate. Fractional contributions of individual isotopomers in each time point were determined as described in the legend to Fig. 7 and are indicated by specific symbols (insets). Lines represent the best fit to a minimal model of hydrogen exchange. Multiplicities are abbreviated as indicated in Fig. 7. Reproduced from (42) with permission of the publisher.

into some relevant metabolites can be dynamically detected in situ by direct ^{13}C MRS or inverse (^{1}H) ^{13}C MRS.

A large number of studies using in vivo ^{13}C MRS has been performed in the intact rodent or human brain. Surface coils constitute the most widespread localization technique, improving the sensitivity and avoiding external interferences (54, 55). ^{13}C MRS 3D localization of a selected volume constituted an important methodological challenge approached by several laboratories during the past decade. Parallel to the development of 3D localization, recent improvements in localized shimming provided an additional contribution to the advance of the technique (56, 57). Both improvements were fundamental to obtain relevant results, opening the field of in vivo ^{13}C MRS as one of the most powerful techniques in noninvasive studies of neurological processes. Contributions from this technology include (i) observation of the natural abundance signals from some brain metabolites in vivo (e.g., myo-inositol) (54); (ii) in situ detection of (1-^{13}C) glycogen in the intact brain (58); and (iii) development of noninvasive studies of cerebral metabolic compartmentation, as ^{13}C labeling of cerebral glutamate and glutamine can be visualized in vivo (57, 59).

More recently, ^{13}C MRS approaches have contributed significantly to our understanding of neuronal-glial interactions in brain (26, 41, 60, 61). A brief
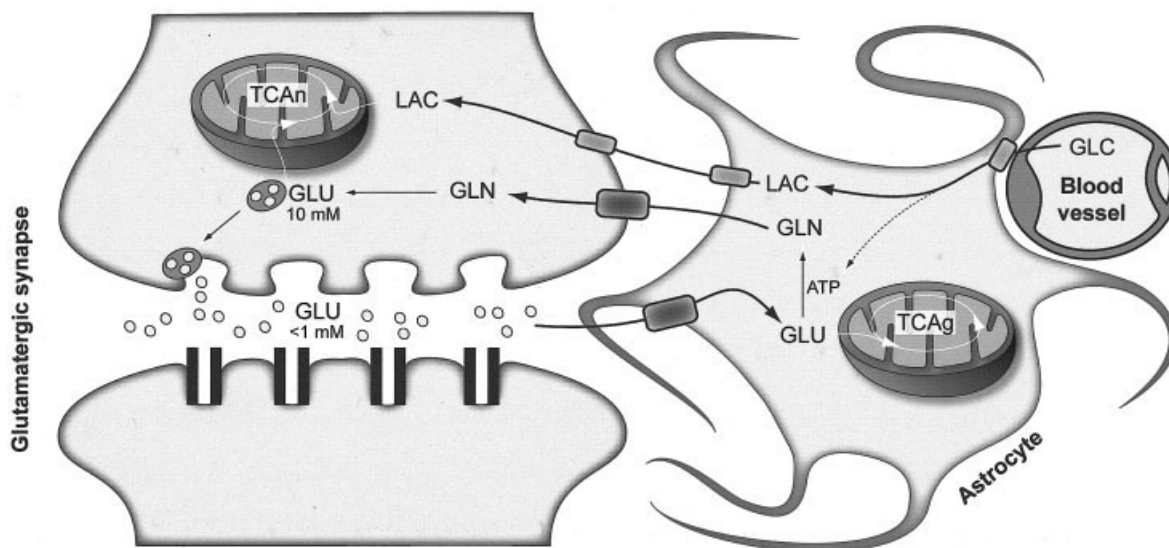
Figure 9 Metabolic coupling between neurons and glia. Glutamatergic neurotransmission releases glutamate from the synaptic vesicles to the synaptic cleft. Synaptic glutamate may be then recaptured by specific astrocyte transporters (together with 3Na$^+$) to produce glutamine through glutamine synthase. Glial glutamine is released to the extracellular space and taken up by neurons, closing the glutamate-glutamine cycle. ATP required for glutamine synthesis (and Na$^+$ extrusion) is produced in the astrocyte by degrading plasma glucose, both oxidatively and nonoxidatively. Thus, glutamatergic neurotransmission is coupled to the intercellular glutamine cycle and astrocytic glucose uptake. GLC: glucose, GLN: glutamine, GLU: glutamate, LAC: lactate, TCAg: glial tricarboxylic acid cycle, TCAn: neuronal tricarboxylic acid cycle.

Table 2   Tricarboxylic Acid Cycle and Glutamate/Glutamine Exchange between the Neuronal Glial Compartments of the Adult Brain as Calculated with Different Models and Methodologies

Process/Model	Garfinkel[a]	Van den Berg and Garfinkel[b]	Kunnecke et al.,[c] Preece and Cerdan[d]	Mason et al.,[e] Sibson et al.,[f,g] Shen et al.,[h] Lebon et al.[i]	Gruetter et al.[k]	Bluml et al.[m]
Total cerebral TCA cycle flux (μmol min^{-1} g^{-1})	1.05	1.5	1.4	1.6 or 0.7,[e] 0.6,[f] 1.0–0.2,[g] 0.8[h]	0.6	0.84
Neuronal TCA cycle flux (μmol min^{-1} g^{-1})	0.40	1.2	1.0	1.6,[e] 0.6,[f] 1.0–0.2,[g] 0.8[h]	0.6	0.70
Glial TCA cycle flux (μmol min^{-1} g^{-1})	0.65	0.3	0.4	0.14[i]		0.14
Size (μmol g^{-1})/turnover (min^{-1}) of large glutamate pool	8.8/21.7	7.0/5.7	5.8/5.8	n.a.		n.a.
Size (μmol g^{-1}) turnover (min^{-1}) of small glutamate pool	1.7/2.6	1.25/4.16	0.5/1.25	n.d./7.7[j]		n.a.
Net transfer of neuronal glutamate to glial compartment (μmol min^{-1} g^{-1})	0.08[n]	0.14	0.1	0.21,[f] 0.40–0.0,[g] 0.32,[h] 0.3[i]	0.3 (0.2)[l]	n.a.
Net transfer of glial glutamine to neuronal compartment (μmol min^{-1} g^{-1})	0.45	n.a.	0.1	0.21,[f] 0.40–0.0,[g] 0.32,[h] 0.3[i]	0.3 (0.2)[l,m]	n.a.

[a] Calculated from specific radioactivity measurements in brain extracts obtained after intracraneal injections of various radioactive precursors including (U-^{14}C) glutamate, (U-^{14}C) aspartate, ^{14}CO$_3$H$^-$, and ^{15}NH$_4$ acetate (69).

[b] Calculated from specific radioactivity measurements in glutamate, glutamine, and aspartate from mouse brain extracts prepared after intraperitoneal injections of ^{14}C-labeled glucose and acetate (70).

[c] Relative flux values were calculated as described in (31) and from the relative ^{13}C isotopomer populations in glutamate, glutamine, and GABA measured by high-resolution ^{13}C NMR in rat brain extracts after infusion of (1,2-^{13}C$_2$) acetate (38).

[d] Absolute flux values were determined from the relative values described in note (c) by measuring the absolute rate of GABA accumulation induced by vigabatrin, a selective inhibitor of GABA transaminase (17).

[e] Determined in vivo from the kinetics of ^{13}C enrichment in glutamate and glutamine C4 carbons from rat or human brain during infusion of (1-^{13}C) glucose, respectively (21, 25).

[f] Determined in vivo from the kinetics of ^{13}C labeling in glutamate and glutamine C4 (55).

[g] Determined in vivo from the kinetics of ^{13}C enrichment in glutamate and glutamine C4, under different conditions of morphine, α-chloralose, and pentobarbital anesthesia (71).

[h] Determined in the human brain in vivo during (1-^{13}C) glucose infusion. Glutamate/glutamine exchange concluded to be stoichiometric 1:1 with CMRglc (72).

[i] Determined in the human brain during metabolism of (2-^{13}C) acetate (73).

[j] Determined in vivo as the inverse of the rate constant of ^{13}C labeling in cerebral glutamate C4 during (1-^{13}C) glucose infusions (74).

[k] Determined in the human brain during (1-^{13}C) glucose infusion with a different model than that used in (f–i) (9).

[l] Only a fraction of glutamine synthesis considered to be derived from neurotransmitter glutamate. Glutamate/glutamine exchange concluded nonstoichiometric with CMRglc, approaching 0.4 rather than the value of 1 concluded in (f–i) (75).

[m] Determined in the human brain during (1-^{13}C) acetate metabolism (76).

[n] Originally proposed as an α-ketoglutarate exchange between the large and small compartments (69).

n.a.: not applicable, n.d.: not detectable.

Adapted from (13). Reproduced with permission of the publisher.

summary is outlined in Fig. 9. Following activation, neurons release glutamate to the synaptic cleft, which either binds to postsynaptic receptors or is recaptured by surrounding astrocytes in the neuropil. Astrocytic glutamate is transformed into glutamine by the ATP-dependent glutamine synthase, glutamine being ex-truded from the astrocyte and recaptured by the neuron. Together, these processes constitute the glutamate-glutamine cycle that underlies the coupling of neuronal and glial metabolisms. The neuronal and glial tricarboxylic acid cycles and the glutamine cycle and been investigated repeatedly by in vivo and in

vitro ^{13}C NMR in a variety of laboratories (*26*, *41*, *60*, *61*).

Table 2 summarizes values for the tricarboxylic acid cycle flux, as obtained using different in vivo ^{13}C NMR approaches compared with earlier radioactive isotope techniques and in vitro ^{13}C isotopomer approaches. In general, tricarboxylic acid cycle fluxes calculated for the adult rat brain were in the range $1.4-0.5$ μmol $\cdot$ min^{-1} $\cdot$ g^{-1}, depending on the mathematical model used for the calculation and the degree of anesthesia. Values found in rodent brain were larger than in humans. Table 2 also shows sizes and turnover rates of the glutamate compartments associated to the "large" and "small" glutamate pools. No direct measurements exist to our knowledge of these pool sizes. The values shown are based on the assumption that the small glutamate pool accounts for approximately 10% of total cerebral glutamate during (1-^{13}C) glucose metabolism. Recent evidences indicate that the relative sizes and fractional ^{13}C enrichments of the large and small glutamate pools could depend on the substrate used (*40*).

An area of promising development is the clinical use of ^{13}C MRS. The high cost of the MRS equipment and ^{13}C isotopes needed for human studies have restricted the use of human ^{13}C MRS to a small number of laboratories. Despite this, several brain disorders have been investigated using ^{13}C MRS, which has already provided new and important clues to clinical diagnosis. The following physiopathological processes have been investigated: (i) in vivo rate of NAA synthesis (*62*); (ii) elucidation of mitochondrial brain disorders (*63*); (iii) the glutamate-glutamine cycle and glutamate neurotransmission in certain diseases (*64*); and (iv) study of hepatic encephalopathy and impaired consciousness (*65*). Additional reviews describing these topics in more detail can be found in (*66–68*).

CONCLUSION

The results obtained in the past two decades have shown that even with a simple ^{13}C MRS methodology and using conventional substrates such as (1,2-^{13}C$_2$) glucose and (1,2-^{13}C$_2$) acetate, it is possible to determine quantitatively metabolic flux through important metabolic pathways in vivo and in vitro. The use of heteronuclear labeling strategies and the increasing power of the associated mathematical modeling may increase significantly the number of pathways amenable to quantitative analysis by ^{13}C MRS in the near future. Finally, ^{13}C MRS will still need to overcome some important challenges. Among these are the study of intracellular α-ketoglutarate/glutamate, the

study of regional metabolism in different brain areas, the quantitative study of neuronal-glial interactions and their alteration in different pathologies, the development microscopic ^{13}C MRS approaches to unravel metabolism in a single cell, and the routine application of in vivo ^{13}C MRS to clinical studies.

REFERENCES

1. Eakin RT, Morgan LO, Gregg CT, Matwiyoff NA. 1972. Carbon-13 nuclear magnetic resonance spectroscopy of living cells and their metabolism of a specifically labeled ^{13}C substrate. FEBS Lett 28(3):259–264.
2. Cerdan S, Seelig J. 1990. NMR studies of metabolism. Annu Rev Biophys Biophys Chem 19:43–67.
3. Kunnecke B. 1995. In carbon-13 NMR spectroscopy of biological systems. In: Beckman N. New York: Academic Press pp 159–267.
4. Morris P, Bachelard H. 2003. Reflections on the application of C-13-MRS to research on brain metabolism. NMR Biomed 16(6–7):303–312.
5. Szyperski T. 1998. ^{13}C-NMR, MS and metabolic flux balancing in biotechnology research. Q Rev Biophys 31(1):41–106.
6. Friebolin H. 1991. Basic one- and two-dimensional NMR spectroscopy. Weinheim: VCH Publishers.
7. Canioni P, Alger JR, Shulman RG. 1983. Natural abundance carbon-13 nuclear magnetic resonance spectroscopy of liver and adipose tissue of the living rat. Biochemistry 22(21):4974–4980.
8. Dobbins RL, Malloy CR. 2003. Measuring in-vivo metabolism using nuclear magnetic resonance. Curr Opin Clin Nutr Metab Care 6(5):501–509.
9. Gruetter R. 2002. In vivo ^{13}C NMR studies of compartmentalized cerebral carbohydrate metabolism. Neurochem Int 41(2–3):143–154.
10. Shulman RG, Rothman DL. 2001. ^{13}C NMR of intermediary metabolism: Implications for systemic physiology. Annu Rev Physiol 63:15–48.

11. Cox IJ. 1996. Development and applications of in vivo clinical magnetic resonance spectroscopy. Prog Biophys Mol Biol 65(1–2):45–81.

12. Jucker BM, Lee JY, Shulman RG. 1998. In vivo ^{13}C NMR measurements of hepatocellular tricarboxylic acid cycle flux. J Biol Chem 273(20):12187–12194.

13. Cruz F, Cerdan S. 1999. Quantitative C-13 NMR studies of metabolic compartmentation in the adult mammalian brain. NMR Biomed 12(7):451–462.

14. Sonnewald U, Schousboe A, Qu H, Waagepetersen HS. 2004. Intracellular metabolic compartmentation assessed by ^{13}C magnetic resonance spectroscopy. Neurochem Int 45(2–3):305–310.

15. Zwingmann C, Leibfritz D. 2003. Regulation of glial metabolism studied by C-13-NMR. NMR Biomed 16(6–7):370–399.

16. Breitmaier E, Voelter W. 1987. Carbon-13 NMR spectroscopy. High-resolution methods and applications in organic chemistry and biochemistry. Weinheim: VCH Publishers.

17. Preece NE, Cerdan S. 1996. Metabolic precursors and compartmentation of cerebral GABA in vigabatrin-treated rats. J Neurochem 67(4):1718–1725.

18. Hu H, Shaka AJ. 1999. Composite pulsed field gradients with refocused chemical shifts and short recovery time. J Magn Reson 136(1):54–62.

19. van de Ven FJM. 1995. Multidimensional NMR in liquids. Basic principles and experimental methods. Weinheim: VCH Publishers.

20. Rothman DL, Behar KL, Hetherington HP, den Hollander JA, Bendall MR, Petroff OA, Shulman RG. 1985. ^{1}H-Observe/^{13}C-decouple spectroscopic measurements of lactate and glutamate in the rat brain in vivo. Proc Natl Acad Sci USA 82(6):1633–1637.

21. Mason GF, Behar KL, Rothman DL, Shulman RG. 1992. NMR determination of intracerebral glucose concentration and transport kinetics in rat brain. J Cereb Blood Flow Metab 12(3):448–455.

22. Burgess SC, Carvalho RA, Merritt ME, Jones JG, Malloy CR, Sherry AD. 2001. ^{13}C isotopomer analysis of glutamate by J-resolved heteronuclear single quantum coherence spectroscopy. Anal Biochem 289(2):187–195.

23. Post JF, Baum E, Ezell EL. 1992. ^{13}C NMR studies of glucose metabolism in human leukemic CEM-C7 and CEM-C1 cells. Magn Reson Med 23(2):356–366.

24. Beckmann N, Turkalj I, Seelig J, Keller U. 1991. ^{13}C NMR for the assessment of human brain glucose metabolism in vivo. Biochemistry 30(26):6362–6366.

25. Mason GF, Gruetter R, Rothman DL, Behar KL, Shulman RG, Novotny EJ. 1995. Simultaneous determination of the rates of the TCA cycle, glucose utilization, alpha-ketoglutarate/glutamate exchange, and glutamine synthesis in human brain by NMR. J Cereb Blood Flow Metab 15(1):12–25.

26. Rothman DL, Behar KL, Hyder F, Shulman RG. 2003. In vivo NMR studies of the glutamate neurotransmitter flux and neuroenergetics: implications for brain function. Annu Rev Physiol 65:401–427.

27. Chance EM, Seeholzer SH, Kobayashi K, Williamson JR. 1983. Mathematical analysis of isotope labeling in the citric acid cycle with applications to 13C NMR studies in perfused rat hearts. J Biol Chem 258(22): 13785–13794.

28. Cruz F, Villalba M, Garcia-Espinosa MA, Ballesteros P, Bogonez E, Satrustegui J, Cerdan S. 2001. Intracellular compartmentation of pyruvate in primary cultures of cortical neurons as detected by ^{13}C NMR spectroscopy with multiple ^{13}C labels. J Neurosci Res 66(5): 771–781.

29. Portais JC, Schuster R, Merle M, Canioni P. 1993. Metabolic flux determination in C6 glioma cells using carbon-13 distribution upon [1-^{13}C]glucose incubation. Eur J Biochem 217(1):457–468.

30. Jeffrey FM, Storey CJ, Sherry AD, Malloy CR. 1996. ^{13}C isotopomer model for estimation of anaplerotic substrate oxidation via acetyl-CoA. Am J Physiol 271(4 Pt 1):E788–799.

31. Kunnecke B, Cerdan S, Seelig J. 1993. Cerebral metabolism of [1,2-^{13}C$_2$]glucose and [U-^{13}C$_4$]3-hydroxy-butyrate in rat brain as detected by ^{13}C NMR spectroscopy. NMR Biomed 6(4):264–277.

32. Malloy CR, Sherry AD, Jeffrey FM. 1990. Analysis of tricarboxylic acid cycle of the heart using ^{13}C isotope isomers. Am J Physiol 259(3, Pt 2):H987–995.

33. Sherry AD, Zhao P, Wiethoff AJ, Jeffrey FM, Malloy CR. 1998. Effects of aminooxyacetate on glutamate compartmentation and TCA cycle kinetics in rat hearts. Am J Physiol 274(2 Pt 2):H591–599.

34. Yu X, White LT, Alpert NM, Lewandowski ED. 1996. Subcellular metabolite transport and carbon isotope kinetics in the intramyocardial glutamate pool. Biochemistry 35(21):6963–6968.

35. Yu X, White LT, Doumen C, Damico LA, LaNoue KF, Alpert NM, Lewandowski ED. 1995. Kinetic analysis of dynamic ^{13}C NMR spectra: Metabolic flux, regulation, and compartmentation in hearts. Biophys J 69(5): 2090–2102.

36. Chatham JC, Forder JR, Glickson JD, Chance EM. 1995. Calculation of absolute metabolic flux and the elucidation of the pathways of glutamate labeling in perfused rat heart by ^{13}C NMR spectroscopy and non-linear least squares analysis. J Biol Chem 270(14): 7999–8008.

37. Cerdan S, Kunnecke B, Seelig J. 1990. Cerebral metabolism of [1,2-^{13}C$_2$]acetate as detected by in vivo and in vitro ^{13}C NMR. J Biol Chem 265(22):12916–12926.

38. Chapa F, Kunnecke B, Calvo R, Escobar del Rey F, Morreale de Escobar G, Cerdan S. 1995. Adult-onset hypothyroidism and the cerebral metabolism of (1,2-^{13}C$_2$) acetate as detected by ^{13}C nuclear magnetic resonance. Endocrinology 136(1):296–305.

39. Pascual JM, Carceller F, Roda JM, Cerdan S. 1998. Glutamate, glutamine, and GABA as substrates for the neuronal and glial compartments after focal cerebral

ischemia in rats. Stroke 29(5):1048–1056; discussion 1056–1047.

40. Chapa F, Cruz F, Garcia-Martin ML, Garcia-Espinosa MA, Cerdan S. 2000. Metabolism of (1-^{13}C) glucose and (2-^{13}C, 2-^{2}H$_3$) acetate in the neuronal and glial compartments of the adult rat brain as detected by (^{13}C, ^{2}H) NMR spectroscopy. Neurochem Int 37(2–3):217–228.

41. Garcia-Espinosa MA, Rodrigues TB, Sierra A, Benito M, Fonseca C, Gray HL, Bartnik BL, Garcia-Martin ML, Ballesteros P, Cerdan S. 2004. Cerebral glucose metabolism and the glutamine cycle as detected by in vivo and in vitro ^{13}C NMR spectroscopy. Neurochem Int 45(2–3):297–303.

42. Garcia-Martin ML, Garcia-Espinosa MA, Ballesteros P, Bruix M, Cerdan S. 2002. Hydrogen turnover and subcellular compartmentation of hepatic [2-^{13}C]glutamate and [3-^{13}C]aspartate as detected by ^{13}C NMR. J Biol Chem 277(10):7799–7807.

43. Moldes M, Cerdan S, Erhard P, Seelig J. 1994. ^{1}H-^{2}H exchange in the perfused rat liver metabolizing [3-^{13}C]alanine and ^{2}H$_2$O as detected by multinuclear NMR spectroscopy. NMR Biomed 7(6):249–262.

44. Lapidot A, Gopher A. 1997. Quantitation of metabolic compartmentation in hyperammonemic brain by natural abundance ^{13}C-NMR detection of ^{13}C-^{15}N coupling patterns and isotopic shifts. Eur J Biochem 243(3):597–604.

45. Preece NE, Cerdan S. 1993. Determining ^{15}N to ^{14}N ratios in biofluids by single-pulse ^{1}H nuclear magnetic resonance. Anal Biochem 215(2):180–183.

46. Clarke DD, Lajhta AL, Maker HS. 1989. Intermediary metabolism. In: Siegel G, Agranoff B, Albers RW, Molinoff P, editors. Basic neurochemistry, Vol. 1. New York: Raven Press pp 541–564.

47. Lapidot A, Gopher A. 1994. Cerebral metabolic compartmentation. Estimation of glucose flux via pyruvate carboxylase/pyruvate dehydrogenase by ^{13}C NMR isotopomer analysis of D-[U-^{13}C]glucose metabolites. J Biol Chem 269(44):27198–27208.

48. Malloy CR, Sherry AD, Jeffrey FM. 1987. Carbon flux through citric acid cycle pathways in perfused heart by ^{13}C NMR spectroscopy. FEBS Lett 212(1):58–62.

49. Cruz F, Scott SR, Barroso I, Santisteban P, Cerdan S. 1998. Ontogeny and cellular localization of the pyruvate recycling system in rat brain. J Neurochem 70(6):2613–2619.

50. García-Martín ML, Ballesteros P, Cerdan S. 2001. The metabolism of water in cells and tissues as detected by NMR methods. Prog NMR Spectrosc 39:41–77.

51. Hansen PE. 1983. Isotope effects on nuclear shielding. Ann Rep NMR Spectrosc 15:105–234.

52. Rodrigues TB, Gray HL, Benito M, Garrido S, Sierra A, Geraldes CF, Ballesteros P, Cerdan S. 2005. Futile cycling of lactate through the plasma membrane of C6 glioma cells as detected by (^{13}C, ^{2}H) NMR. J Neurosci Res 79(1–2):119–127.

53. Dziembowska T, Hansen PE, Rozwadowski Z. 2004. Studies based on deuterium isotope effect on ^{13}C chemical shifts. Prog Nucl Magn Reson Spectrosc 45:1–29.

54. Gruetter R, Rothman DL, Novotny EJ, Shulman RG. 1992. Localized ^{13}C NMR spectroscopy of myo-inositol in the human brain in vivo. Magn Reson Med 25(1):204–210.

55. Sibson NR, Dhankhar A, Mason GF, Behar KL, Rothman DL, Shulman RG. 1997. In vivo ^{13}C NMR measurements of cerebral glutamine synthesis as evidence for glutamate-glutamine cycling. Proc Natl Acad Sci U S A 94(6):2699–2704.

56. Gruetter R, Boesch C. 1992. Fast, noniterative shimming of spatially localized signals—in vivo analysis of the magnetic-field along axes. J Magn Reson 96(2):323–334.

57. Gruetter R. 1993. Automatic, localized in vivo adjustment of all first- and second-order shim coils. Magn Reson Med 29(6):804–811.

58. Choi IY, Tkac I, Gruetter R. 2000. Single-shot, three-dimensional "non-echo" localization method for in vivo NMR spectroscopy. Magn Reson Med 44(3):387–394.

59. Gruetter R, Novotny EJ, Boulware SD, Mason GF, Rothman DL, Shulman GI, Prichard JW, Shulman RG. 1994. Localized ^{13}C NMR spectroscopy in the human brain of amino acid labeling from D-[1-^{13}C]glucose. J Neurochem 63(4):1377–1385.

60. Rodrigues TB, Cerdan S. 2005. The cerebral tricarboxylic acid cycles. In: Gibson G, Dienel D, editors. Neural energy utilization, Vol. 5. Handbook of neurochemistry and molecular neurobiology. 3rd ed. New York: Kluwer Academic/Plenum. In press.

61. Sierra A, Rodrigues TB, Benito M, Ballesteros P, Garcia-Espinosa MA, Garcia-Martin ML, Cerdan S. 2005. Pyruvate oxidation and mitochondrial substrate transport in the central nervous system. In: Gruetter R, editor. Neural metabolism in vivo, Vol. 4. Handbook of neurochemistry and molecular neurobiology. 3rd ed. New York: Kluwer Academic/Plenum Publisher. In press.

62. Moreno A, Ross BD, Bluml S. 2001. Direct determination of the N-acetyl-L-aspartate synthesis rate in the human brain by ^{13}C MRS and [1-^{13}C]glucose infusion. J Neurochem 77(1):347–350.

63. Bluml S, Moreno A, Hwang JH, Ross BD. 2001. 1-^{13}C glucose magnetic resonance spectroscopy of pediatric and adult brain disorders. NMR Biomed 14(1):19–32.

64. Lin AP, Shic F, Enriquez C, Ross BD. 2003. Reduced glutamate neurotransmission in patients with Alzheimer's disease—an in vivo ^{13}C magnetic resonance spectroscopy study. Magma 16(1):29–42.

65. Bluml S, Moreno-Torres A, Ross BD. 2001. [1-^{13}C]glucose MRS in chronic hepatic encephalopathy in man. Magn Reson Med 45(6):981–993.

66. Gruetter R, Adriany G, Choi IY, Henry PG, Lei HX, Oz GL. 2003. Localized in vivo C-13 NMR spectroscopy of the brain. NMR Biomed 16(6–7):313–338.

67. de Graaf RA, Mason GF, Patel AB, Behar KL, Roth-

man DL. 2003. In vivo ^{1}H-[^{13}C]-NMR spectroscopy of cerebral metabolism. NMR Biomed 16(6–7):339–357.

68. Ross B, Lin A, Harris K, Bhattacharya P, Schweinsburg B. 2003. Clinical experience with C-13 MRS in vivo. NMR Biomed 16(6–7):358–369.

69. Garfinkel D. 1966. A simulation study of the metabolism and compartmentation in brain of glutamate, aspartate, the Krebs cycle, and related metabolites. J Biol Chem 241(17):3918–3929.

70. van den Berg CJ, Garfinkel D. 1971. A stimulation study of brain compartments. Metabolism of glutamate and related substances in mouse brain. Biochem J 123(2):211–218.

71. Sibson NR, Dhankhar A, Mason GF, Rothman DL, Behar KL, Shulman RG. 1998. Stoichiometric coupling of brain glucose metabolism and glutamatergic neuronal activity. Proc Natl Acad Sci U S A 95(1): 316–321.

72. Shen J, Shungu DC, Rothman DL. 1999. In vivo chemical shift imaging of gamma-aminobutyric acid in the human brain. Magn Reson Med 41(1):35–42.

73. Lebon V, Petersen KF, Cline GW, Shen J, Mason GF, Dufour S, Behar KL, Shulman GI, Rothman DL. 2002. Astroglial contribution to brain energy metabolism in humans revealed by ^{13}C nuclear magnetic resonance spectroscopy: Elucidation of the dominant pathway for neurotransmitter glutamate repletion and measurement of astrocytic oxidative metabolism. J Neurosci 22(5): 1523–1531.

74. Mason GF, Rothman DL, Behar KL, Shulman RG. 1992. NMR determination of the TCA cycle rate and alpha-ketoglutarate/glutamate exchange rate in rat brain. J Cereb Blood Flow Metab 12(3):434–447.

75. Gruetter R, Seaquist ER, Ugurbil K. 2001. A mathe-matical model of compartmentalized neurotransmitter metabolism in the human brain. Am J Physiol Endocrinol Metab 281(1):E100–112.

76. Bluml S, Moreno-Torres A, Shic F, Nguy CH, Ross BD. 2002. Tricarboxylic acid cycle of glia in the in vivo human brain. NMR Biomed 15(1):1–5.

BIOGRAPHIES

Tiago B. Rodrigues graduated as a biochemist from the University of Coimbra, Portugal, in 2000. In 2001, he visited the Mary Nell and Ralph B. Rogers Magnetic Resonance Center at the University of Texas Southwestern Medical Center at Dallas where he investigated the Ca^{2+} regulation of the tricarboxylic acid cycle by ^{13}C isotopomer kinetic analysis. Since 2002, he has been a Ph.D. student at the University of Coimbra and also developing the lab work in the Institute of Biomedical Research "Alberto Sols" CSIC/UAM. His research is focused on lactate turnover in neural cells and transformed cell lines as monitored with double isotope-labeled NMR methodologies.

Sebastián Cerdán is the Director of the Institute of Biomedical Research "Alberto Sols" CSIC/UAM as well as the Laboratory for Imaging and Spectroscopy by Magnetic Resonance. He has contributed a variety of ^{13}C NMR and multiple-isotope approaches to hepatic and cerebral metabolisms since the early 1980s. His current main interests involve the study of metabolic compartmentation in liver or brain and the development of fast hydrogen turnover measurements to investigate intercellular and subcellular lactate and glutamate metabolisms in these organs.